Ceramics International 44 (2018) 12934–12939

Contents lists available at ScienceDirect

Ceramics International

journal homepage: www.elsevier.com/locate/ceramint

Supersonically sprayed clay, silica, and silica aerogel hybrid films as thermal and electrical barriers

Tae-Gun Kim[a,1], Chan-Woo Park[a,1], Jong-Gun Lee[a], Min-Woo Kim[a], Mun Seok Choi[b], Woo Yeong Kim[b], Jae Sin Yang[b], Sam S. Yoon[a,*]

[a] School of Mechanical Engineering, Korea University, Seoul 02841, Republic of Korea
[b] MS AUTOTECH, 1023 Nogokli, Nanamyun, Gyungju 780-851, Republic of Korea

ARTICLE INFO

Keywords:
Thermal barrier coating
Supersonic spray
Clay
SiO_2
Aerogel
Heating
Cooling

ABSTRACT

A thermal barrier coating (TBC) provides protection from thermal damage. While sufficiently thick coatings facilitate thermal protection, space limitations often require the use of high-performing barrier materials, such as clays, silica, and aerogels. Herein, we demonstrate the fabrication of thin TBCs of clay, silica, and silica aerogel microparticles deposited by supersonic cold spraying. The coated films were characterized by scanning electron microscopy and transmission electron microscopy. The effects of varied coating thicknesses from 1 to 5 mm on the TBC performance of each material were studied for both heating and cooling scenarios. We found that the hybrid clay–aerogel coating provided the best thermal insulation. Deposition by supersonic cold spraying is rapid and scalable, with potential applicability for the commercial production of TBCs.

1. Introduction

Thermal barrier coatings (TBCs) are widely used to protect diesel engines and high-pressure turbines to prolong the lifespans of their components [1,2]. TBCs were initially enamel coatings applied to military engine components in the early 1950s; since then, Al_2O_3 [3], ZrO_2 [4], and yttria-stabilized ZrO_2 (YSZ) [4] have become popular materials for thermal protection and insulation. The materials used for TBCs must satisfy several requirements: (1) low thermal diffusivity, (2) minimal phase change under high temperatures, (3) strong adhesion to the target substrate, and (4) resistance to oxidation and corrosion [5].

Electron-beam physical vapor deposition (EB-PVD) [1,4] and atmospheric plasma spraying (APS) [3,6,7] are used to deposit TBCs. EB-PVD is primarily used for dynamic components like turbine blades, which are subject to both thermal and mechanical loadings. Porous structures are often intentionally designed for TBC layers to enhance their thermal insulating performance. APS, an alternative lower-cost method, has been the subject of significant research intended to improve the thermal insulation performance of deposited materials. APS is typically used for static components like combustor cans and vane platforms, as opposed to EB-PVD, which is more appropriate for dynamic components subject to mechanical fatigue [8]. In general, APS coatings comprise two layers: a ceramic layer for thermal protection and a metal layer used to bond the ceramic and substrate.

Supersonic cold spraying can be used to apply insulating materials without using plasma or an electron beam. The operational costs of supersonic cold spraying are much lower than those of either EB-PVD or APS, because supersonic cold spraying only requires the heating of pressurized air without any additional expensive components. Supersonic microparticles are deposited onto either rigid or flexible substrates and adhered using only their kinetic energy. The simplicity and low cost of supersonic cold spraying are highly attractive compared to the complexity and expense of EB-PVD and APS.

We have previously demonstrated the use of various clays for thermal insulation [9]. However, the use of other insulating materials, such as silica and aerogels, has not yet been studied with supersonic cold spraying. Silica-aerogel, a superior insulating material, consists of more than 90% of air and less than 10% of solid silica by volume [10,11]. While solid silica powder has been supersonically sprayed into insulating layers, silica aerogel (henceforth “aerogel”) has not been tested in coating via supersonic spraying [12]. Aerogel is a highly porous material with low density, low thermal conductivity, and low thermal diffusivity [13]. These advantages suggest promising thermal insulating performance for supersonically sprayed mixtures of clay, silica, and aerogel. The rapidity and low cost of supersonic cold spraying indicate its applicability for commercial implementation.

Herein, we demonstrate the fabrication of a large-scale flexible insulating tape coated with aerogel and clay particles via supersonic cold

* Corresponding author.
E-mail address: skyoon@korea.ac.kr (S.S. Yoon).
[1] Equal contribution

https://doi.org/10.1016/j.ceramint.2018.04.106
Received 16 March 2018; Received in revised form 30 March 2018; Accepted 12 April 2018
Available online 17 April 2018

Table 1
Operating conditions for supersonic cold spraying.

Conditions	
Pressure [bar]	2
Gas preheating temperature [°C]	250
Traverse speed [mm/s]	40
Nozzle-to-substrate distance [mm]	50

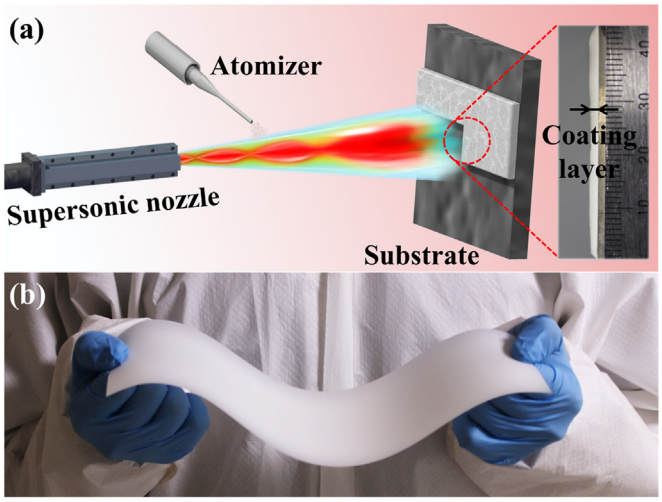

Fig. 1. (a) Supersonic spray schematic. (b) Large-scale flexible insulating tape coated with clay (montmorillonite) and aerogel microparticles.

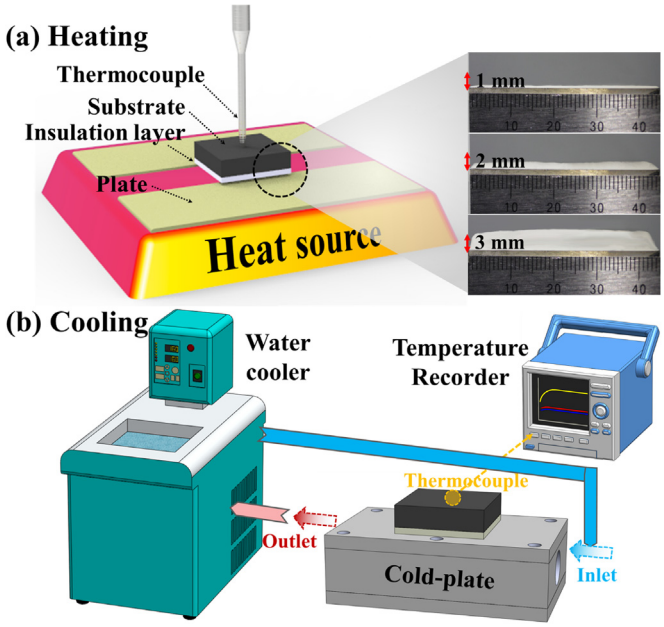

Fig. 2. (a) Schematic of the experimental setup comprising heater, insulation layer, stainless steel substrate, and thermocouple. (Insets) Coatings of various thicknesses made up of montmorillonite, silica, and aerogel microparticles. (b) Schematic of the cooling system. Cold water is supplied to the heat-exchange system and the heated water returns to the chiller.

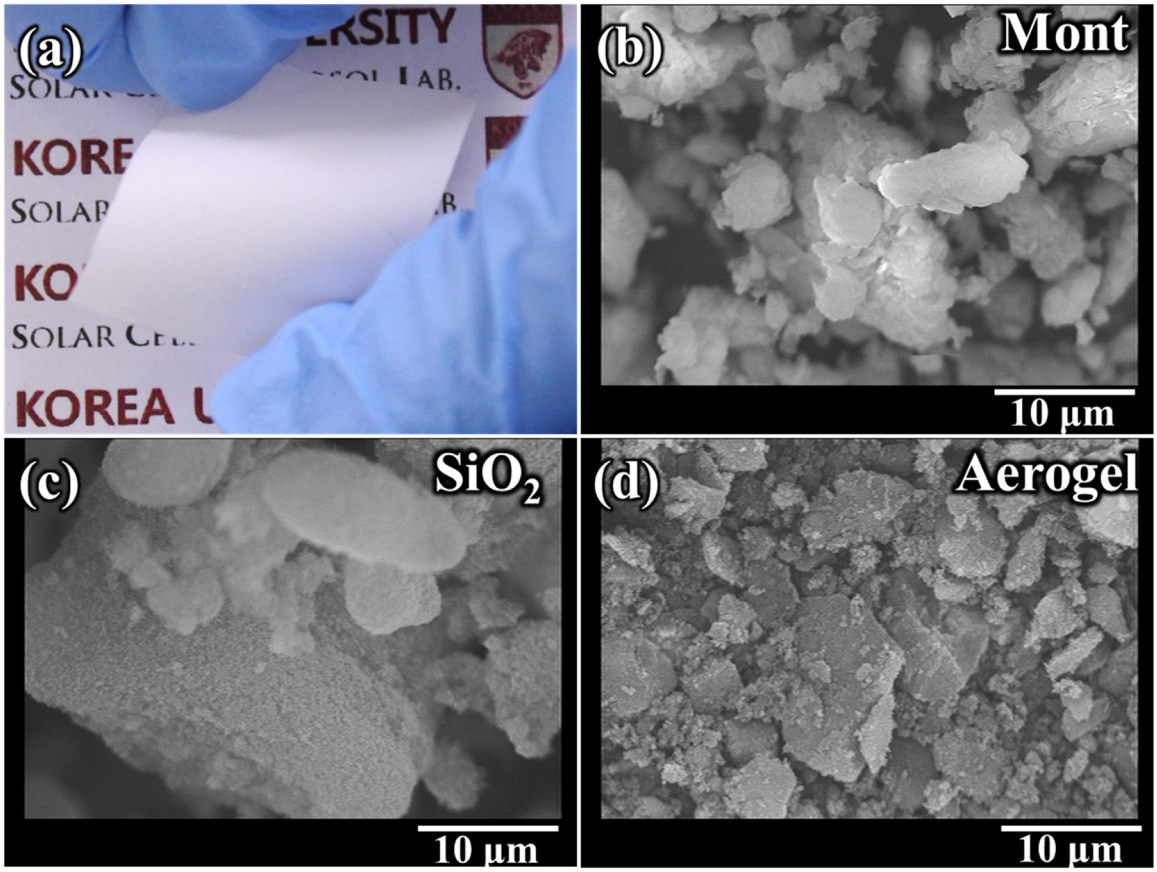

Fig. 3. (a) A photograph of flexible, supersonically sprayed montmorillonite–aerogel insulating films. (b) SEM images of montmorillonite, silica, and aerogel microparticles.

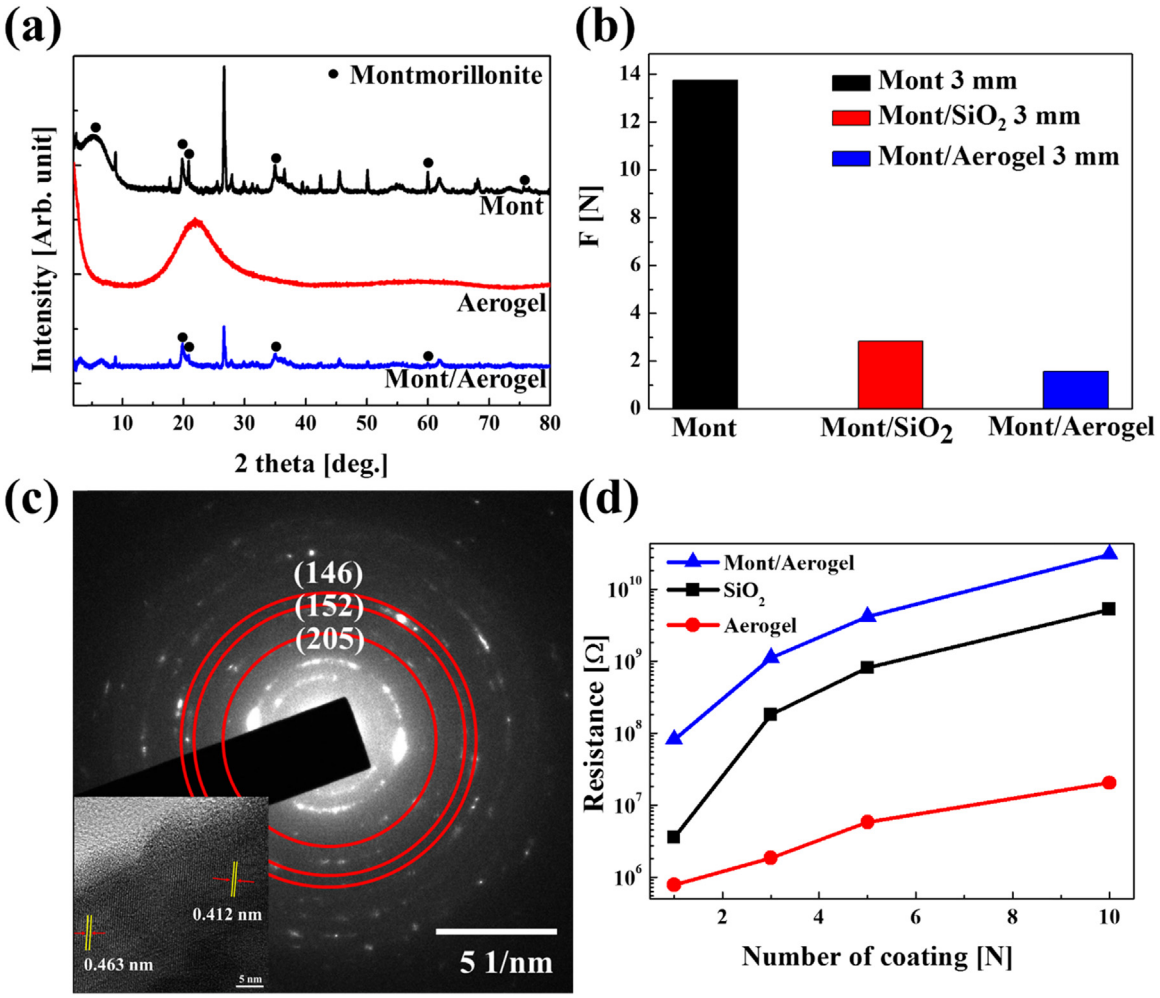

Fig. 4. (a) XRD spectra of aerogel, montmorillonite, and montmorillonite–aerogel hybrid. (b) Adhesion tests of hybrid montmorillonite films. (c) SAED pattern and HR-TEM image of the montmorillonite film. (d) Electrical resistivity test.

spraying. The coated layers are materially characterized and the thermal insulation performances of the hybrid coatings are compared and quantified.

2. Experimental methods

2.1. Fabrication of thermal insulation layer

All thermal insulation layers were produced using a supersonic cold spraying apparatus, comprising a supersonic nozzle, atomizer, gas heater, syringe pump, and *x*–*y* motor stage. The detailed operating conditions for the supersonic cold spraying process are summarized in Table 1. Fig. 1**a** shows the supersonic spray nozzle, which produces a supersonic stream of the working fluid containing the microparticles. The microparticle-laden fluid issues from an atomizer (VCS 40 kHz, Sonics & Materials) at a flow rate of 3.0 mL/min using a syringe pump (Legato 210, KDS). Upon the evaporation of the fluid, the microparticles form a coating layer. The substrates used in this study were stainless steel (SKD61) and flexible polyethylene terephthalate (PET). The insulation layer thickness was controlled by changing the number of sweeps by the *x*–*y* stage. Details of the supersonic spraying process are available in our previous work [14–17]. Fig. 1**b** depicts a large, flexible coating of clay (montmorillonite) and aerogel microparticles, demonstrating the scalability and rapid production capability of the supersonic cold spraying process.

2.2. Solution preparation

Insulating materials include montmorillonite (Mont., Surface area 250 m^2/g, Sigma Aldrich), silica (SiO_2, 10–20 nm, Sigma Aldrich), and silica aerogel (~10–100 μm, 0.016 < *k* < 0.019 W/m·K at 25 °C, REM Tech, Korea) microparticles. Montmorillonite microparticles (7.5 g) were dispersed in 50 mL of isopropyl alcohol (IPA, Duksan, Korea) with 0.25 g of nylon to prepare a colloidal precursor. The volume ratio of montmorillonite to silica or aerogel microparticles was 2:1. More montmorillonite was used to promote adhesion between the microparticles and substrate; montmorillonite showed good substrate adhesion, while the silica and aerogel tended to detach from the substrate because of their sharp and irregular particle shapes. The mixed solution was then sonicated for 90 s to disperse the microparticles.

2.3. Hot plate system

Fig. 2**a** depicts the experimental setup used to evaluate the thermal insulation performances of the fabricated coatings. The insulation layer is first deposited on a stainless steel substrate and then placed on a heated plate at 800 °C, as illustrated in Fig. 2**a**. A *K*-type thermocouple is placed on the surface of the substrate. The inset in Fig. 2**a** shows the deposited insulation layers of various thicknesses. Fig. 2**b** shows the experimental setup for the cooling test. The cold plate was chilled with cooling water (10 ± 0.5 °C) from a chiller (Lab Companion, RW-0525 G) and then recycled. The temperature (within ± 0.1 °C error) of

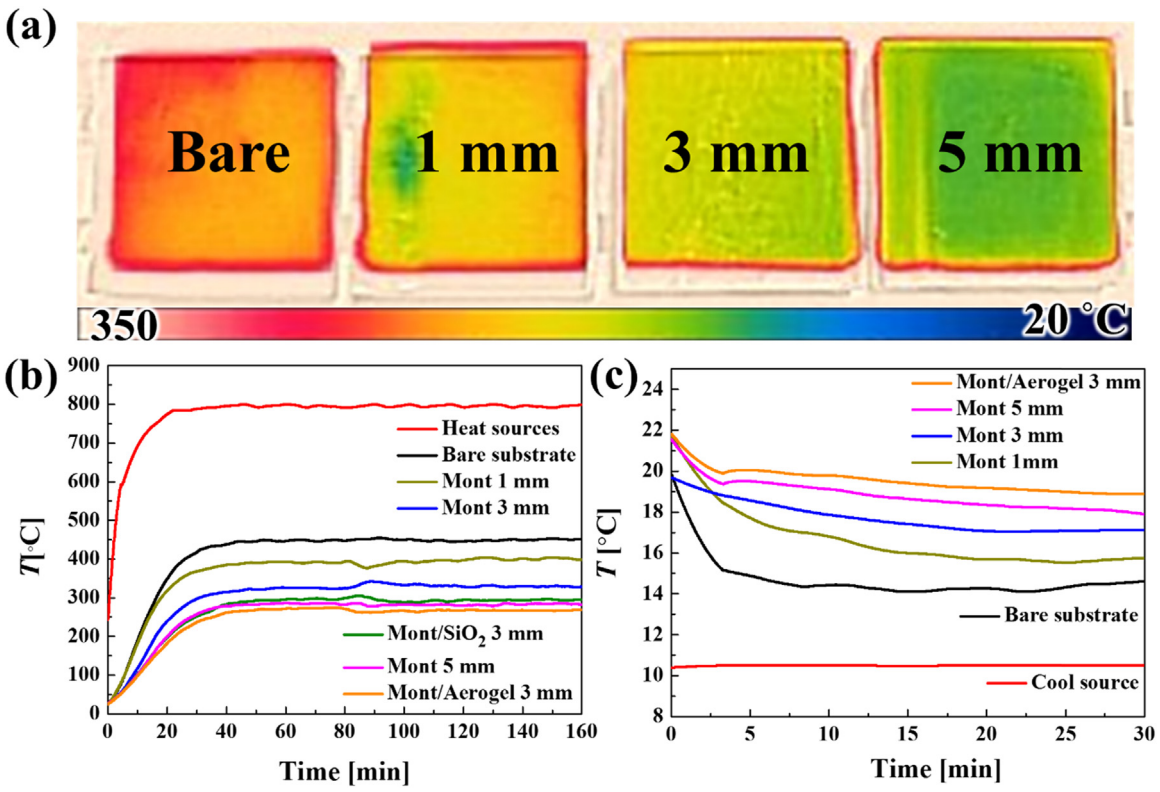

Fig. 5. Thermal responses of the insulating coatings of various thicknesses. (a) Temperature distributions from the IR camera. (b) The steady-state temperature for each coating during heating processes. (c) Cooling processes as a function of material and thickness.

the insulating coating was recorded every 0.25 s with a *K*-type thermocouple.

2.4. Characterization

The morphologies of montmorillonite, SiO_2, and aerogel particles were characterized using a field-emission scanning electron microscope (FE-SEM, S-5000, Hitachi, Japan) at 10 kV and a transmission electron microscope (TEM, JEM 2100F, JEOL Inc.). X-ray photoelectron spectroscopy (XPS, Theta Probe Base System, Thermo Fisher Scientific Co.) measurements were conducted to evaluate the chemical states of elements of the films. An infrared (IR) camera (FLIR system, Inc. FLIR-E63900) was used to visualize the temperature field. A data logger (GL-240, Graphtec, U.S.) and *K*-type thermocouple (probe size = 1.0 ∅ × 150 mm) measured the temperature changes. Adhesion testing was conducted using a centrifugal adhesion test apparatus (LF 204, Centrifugal Adhesion Testing Technology, Young Jin Corporation, South Korea). The electrical resistivity was measured using a Smartec Insulation & Continuity instrument (MI 3121, < 30 GΩ, Metrel d.d., Slovenia).

3. Results and discussion

Fig. 3**a** demonstrates the superior flexibility of the insulating film of montmorillonite–aerogel particles. Fig. 3**b–d** respectively show SEM images of the morphologies of the montmorillonite, silica, and aerogel microparticles, which range in size from a few to tens of micrometers. The silica particles are generally larger; both silica and aerogel have more angular particle shapes than montmorillonite. Larger, more acutely angled particles are more difficult to deposit; thus, montmorillonite was mixed with these particles at a 2:1 volume ratio to promote adhesion.

The XRD diffraction patterns of the fabricated films are shown in Fig. 4**a**. The sharp peaks in the pattern from the insulating film consisting of montmorillonite and aerogel particles appear at $2\theta = 5.97^\circ$, 20.70°, 21.57°, 35.04°, 44.27°, 47.19°, and 60.25°, corresponding to the (100), (111), (112), (211), (135), (233), and (060) planes of montmorillonite (JCPDS 27–0733). The broad peak of the aerogel powder at $2\theta = 23^\circ$ indicates the amorphous nature of the original silica aerogel [18].

The diffraction peaks of the hybrid fabricated montmorillonite–aerogel film show similarity to those of the clay at $2\theta = 20.70^\circ$, 21.57°, and 60.25°, although the peak intensity is relatively lower.

Fig. 4**b** compares the adhesive strengths of the coated films consisting of montmorillonite and its mixtures with silica and aerogel particles. The aerogel particles are inherently non-adhesive because of their low surface polarity [19]. To improve the adhesive strength, the aerogel was mixed with inherently sticky and adhesive montmorillonite. Fig. 4b shows that the montmorillonite film possesses the highest adhesive strength of. While the hybrid films of montmorillonite–silica and montmorillonite–aerogel exhibit relatively poor adhesive strengths, they are sufficiently adhesive for successful attachment to a substrate.

Fig. 4**c** shows the selected-area electron diffraction (SAED) patterns of the montmorillonite films. The crystalline state of montmorillonite is detected in comparing the diffraction ring pattern of the film with the XRD diffraction pattern in Fig. 4**a**. The inset in Fig. 4**c** shows the high-resolution TEM (HR-TEM) image of the fabricated film, showing the lattice space distances (*d*-spacing). The *d*-spacings between two pairs of parallel yellow lattice fringes are 0.463 and 0.412 nm, corresponding to the (020) and (112) planes of montmorillonite (JCPDS 27-0733), respectively.

Electrical insulation is often important for thermal insulation films intended to protect objects from both heat and electricity. Therefore, Fig. 4**d** compares the electrical resistivities of the fabricated films. In general, montmorillonite, SiO_2, and aerogel are highly resistive to electricity [9]. The number of coating passes *N* refers to the number of nozzle sweep passes, which controls the film thickness; larger *N*

corresponds to a thicker film. The films become more electrically resistive as *N* increases for all three cases. The montmorillonite–aerogel hybrid film has the highest electrical resistance, compared to the pure silica and aerogel films.

Fig. 5 compares the temperature changes of the substrates. Fig. 5**a-b** depict data from the heating experiments, while Fig. 5**c** shows the cooling experiment results, corresponding to Fig. 2**a** and **b**, respectively. The fundamental heat-exchange mechanism for heating and cooling is equivalent. Fig. 5**a** shows IR images of the stainless steel substrate for coating thicknesses of 0 (bare), 1, 3, and 5 mm, taken after 20 min of heating. The IR images indicate that the sample temperatures range from 200 to 350 °C depending on the coating thickness. As expected, the thicker coatings show lower temperatures.

In Fig. 5**b**, the heat source reaches 800 °C after 30 min. Because of ubiquitous thermal resistance, the substrate surface temperature shows a delay that increases with the application of coatings; thicker coatings correspond to more suppressed temperature increases of the substrate surface. The 3-mm-thick hybrid material coatings both outperform the 5-mm-thick pure montmorillonite coating, confirming the superior insulating capability of the hybrid materials comprising montmorillonite mixed with silica or silica aerogel.

Fig. 5**c** also confirms the superior insulation capability of the montmorillonite–aerogel hybrid coating. The cooling water temperature is 10.5 °C and the surface temperature of the bare substrate is about 14 °C. Again, coatings of increasing thickness show progressively better performance. The 3-mm-thick hybrid coating outperforms the pure montmorillonite coating, even that of 5 mm in thickness, because of the superior insulation properties of aerogel.

Silica is a group IV metal oxide that shows good abrasion resistance, electrical insulation, and thermal stability; these useful physical and electronic properties are applied in semiconductor devices [20]. Aerogels are assembled from microparticles or polymer molecules that form a porous medium; 98% of the volume of an aerogel monolith is gas or vacuum. They are the lightest solids in the world, with bulk densities about three times that of air. Aerogels have high specific surface areas, low densities and refractive indices, and microporous structures (pores < 2 mm). The microporosity yields extremely low thermal conductivity [21]. The material and structure of aerogels can minimize thermal conduction and convection, yielding thermal conductivities of only ~13 mW/m K [22]. Aerogels can be classified by preparation method, pore size, or appearance (powder versus film). However, the most common property used to distinguish them is composition, such as oxide aerogels [13], organic aerogels [23], carbon aerogel [24], and other aerogels [25]. Herein, we used an oxide aerogel.

Fig. 6 demonstrates the thermal insulation performance of the insulating coatings through chocolate-melting tests. The bare substrate (0 mm), 3-mm-thick pure montmorillonite, and 3-mm-thick montmorillonite–aerogel coatings were tested by observing chocolate melt. The insulation layers face downward and are located between the lamp flame and the supporting mesh. Alcohol lamps with the flame temperature of 700 °C are used to heat the stainless steel substrates for up to 12 min, during which the chocolate pieces are melted; see **movie S1** in the Supporting Information. The chocolate sample on an uncoated substrate melted at $t = 4$ min; samples on 3-mm pure montmorillonite

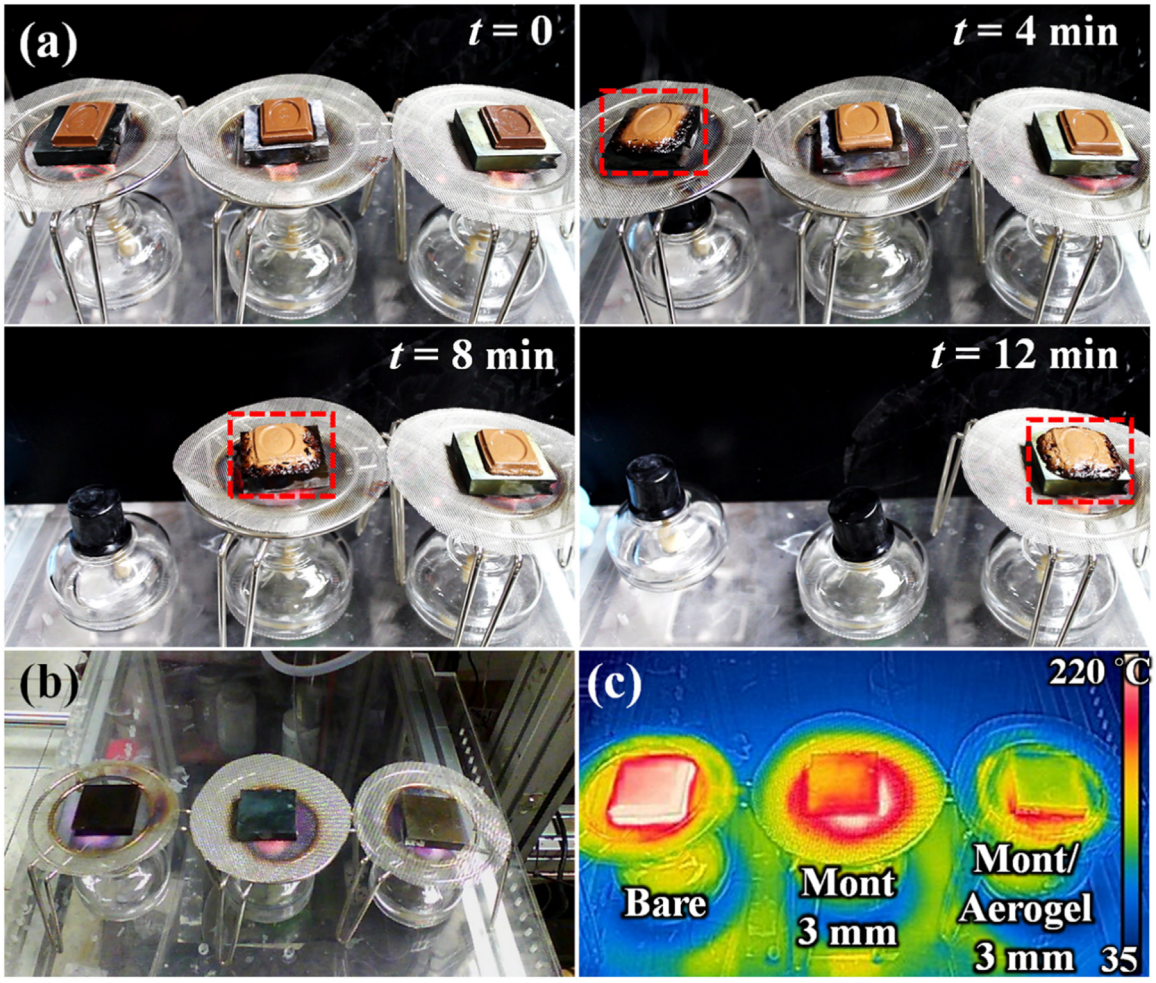

Fig. 6. (a) Thermal responses of coatings during chocolate-melt testing after heating for 12 min (b) The uncoated, pure montmorillonite, and montmorillonite–aerogel surfaces under heat and (c) their corresponding IR thermal images.

and 3-mm montmorillonite–aerogel melted completely at $t = 8$ and 12 min, respectively. This testing confirms that the hybrid coating comprising ⅔ montmorillonite and ⅓ aerogel by volume yields the best insulation performance. The IR image in Fig. 6**c** also confirms the superior insulation capability of the hybrid coating.

Supplementary material related to this article can be found online at http://dx.doi.org/10.1016/j.ceramint.2018.04.106.

4. Conclusions

Montmorillonite, silica, and silica aerogel microparticles were deposited onto rigid stainless steel and flexible PET substrates by supersonic cold spraying. Insulating layers of various thicknesses were tested regarding their performance as thermal barriers. The results showed that the inclusion of 33 vol% silica or silica aerogel yielded improved insulation performance relative to pure montmorillonite coatings, even to those of greater thicknesses. Supersonically sprayed insulating coatings are flexible and readily applicable to complex shapes in confined spaces. In addition, the application process is rapid and scalable, thus demonstrating its commercial potential.

Acknowledgment

This research was supported by MS AUTOTECH. This research was also supported by the Technology Development Program to Solve Climate Changes of the National Research Foundation (NRF) funded by the Ministry of Science, ICT & Future Planning (NRF-2016M1A2A2936760), NRF-2017R1A2B4005639, and NRF-2013R1A5A1073861. This work was also supported by the National Research Council of Science & Technology (NST) grant by the Korea government (MSIP) (No. CRC-16-02-KICT).

References

[1] M. Peters, C. Leyens, U. Schulz, W.A. Kaysser, EB-PVD thermal barrier coatings for aeroengines and gas turbines, Adv. Eng. Mater. 3 (2001) 193–204.
[2] N.P. Padture, M. Gell, E.H. Jordan, Thermal barrier coatings for gas-turbine engine applications, Science 296 (2002) 280–284.
[3] A.M. Limarga, S. Widjaja, T.H. Yip, Mechanical properties and oxidation resistance of plasma-sprayed multilayered Al_2O_3/ZrO_2 thermal barrier coatings, Surf. Coat. Technol. 197 (2005) 93–102.
[4] U. Schulz, Phase transformation in EB-PVD yttria partially stabilized zirconia thermal barrier coatings during annealing, J. Am. Ceram. Soc. 83 (2000) 904–910.
[5] F. Cernuschi, P. Bianchi, M. Leoni, P. Scardi, Thermal diffusivity/microstructure relationship in Y-PSZ thermal barrier coatings, J. Therm. Spray. Technol. 8 (1999) 102–109.
[6] M. Shinozaki, T. Clyne, The effect of vermiculite on the degradation and spallation of plasma sprayed thermal barrier coatings, Surf. Coat. Technol. 216 (2013) 172–177.
[7] J.A. Haynes, M. Ferber, W. Porter, Thermal cycling behavior of plasma-sprayed thermal barrier coatings with various MCrAlX bond coats, J. Therm. Spray. Technol. 9 (2000) 38–48.
[8] A.G. Evans, D. Mumm, J. Hutchinson, G. Meier, F. Pettit, Mechanisms controlling the durability of thermal barrier coatings, Prog. Mater. Sci. 46 (2001) 505–553.
[9] D.-Y. Kim, J.-G. Lee, B. Joshi, J.-H. Lee, S.S. Al-Deyab, H.G. Yoon, D.R. Yang, A. Yarin, S.S. Yoon, Supersonically sprayed thermal barrier layers using clay microparticles, Appl. Clay Sci. 120 (2016) 142–146.
[10] F. Shi, L. Wang, J. Liu, Synthesis and characterization of silica aerogels by a novel fast ambient pressure drying process, Mater. Lett. 60 (2006) 3718–3722.
[11] J.L. Gurav, I.-K. Jung, H.-H. Park, E.S. Kang, D.Y. Nadargi, Silica aerogel: synthesis and applications, J. Nanomater. 2010 (2010) 23.
[12] J.-G. Lee, S. An, T.-G. Kim, M.-W. Kim, H.-S. Jo, M.T. Swihart, A.L. Yarin, S.S. Yoon, Self-cleaning anticondensing glass via supersonic spraying of silver nanowires, silica, and polystyrene nanoparticles, ACS Appl. Mater. Interfaces 9 (2017) 35325–35332.
[13] A.S. Dorcheh, M. Abbasi, Silica aerogel; synthesis, properties and characterization, J. Mater. Process. Technol. 199 (2008) 10–26.
[14] J.-G. Lee, J.-H. Lee, S. An, J.Y. Yoon, J.-W. Choi, M.G. Kang, J.I. Lee, H.-e. Song, S.S. Al-Deyab, S.C. James, Y. Kang, D. Kim, S.S. Yoon, H.-S. Lee, Effects of impact conditions on the electrical and mechanical properties of supersonic cold sprayed Cu–Ni electrodes, J. Alloy. Compd. 695 (2017) 3714–3721.
[15] J.-G. Lee, B.N. Joshi, J.-H. Lee, T.-G. Kim, D.-Y. Kim, S.S. Al-Deyab, I.W. Seong, M.T. Swihart, W.Y. Yoon, S.S. Yoon, Stable high-capacity lithium ion battery anodes produced by supersonic spray deposition of hematite nanoparticles and self-healing reduced graphene oxide, Electrochim. Acta 228 (2017) 604–610.
[16] J.-G. Lee, D.-Y. Kim, T.-G. Kim, J.-H. Lee, S.S. Al-Deyab, H.W. Lee, J.S. Kim, D.H. Yang, A.L. Yarin, S.S. Yoon, Supersonically sprayed copper-nickel microparticles as flexible and printable thin-film high-temperature heaters, Adv. Mater. Interfaces (2017) 1700075.
[17] J.G. Lee, D.Y. Kim, J.H. Lee, S. Sinha-Ray, A.L. Yarin, M.T. Swihart, D. Kim, S.S. Yoon, Production of flexible transparent conducting films of self-fused nanowires via one-step supersonic spraying, Adv. Funct. Mater. 27 (2017).
[18] W. Xu, A. Du, J. Tang, P. Yan, X. Li, Z. Zhang, J. Shen, B. Zhou, Template confined synthesis of Cu-or Cu_2O-doped SiO_2 aerogels from Cu (ii)-containing composites by in situ alcohothermal reduction, RSC Adv. 4 (2014) 49541–49546.
[19] S. Vallon, A. Hofrichter, B. Drevillon, J. Klemberg-Sapieha, L. Martinu, F. Poncin-Epaillard, Improvement of the adhesion of silica layers to polypropylene induced by nitrogen plasma treatment, Thin Solid Films 290 (1996) 68–73.
[20] T. Yamane, N. Nagai, S.-i. Katayama, M. Todoki, Measurement of thermal conductivity of silicon dioxide thin films using a 3ω method, J. Appl. Phys. 91 (2002) 9772.
[21] M. Reim, W. Körner, J. Manara, S. Korder, M. Arduini-Schuster, H.-P. Ebert, J. Fricke, Silica aerogel granulate material for thermal insulation and daylighting, Sol. Energy 79 (2005) 131–139.
[22] J.P. Randall, M.A.B. Meador, S.C. Jana, Tailoring mechanical properties of aerogels for aerospace applications, ACS Appl. Mater. Interfaces 3 (2011) 613–626.
[23] P. Lorjai, T. Chaisuwan, S. Wongkasemjit, Porous structure of polybenzoxazine-based organic aerogel prepared by sol–gel process and their carbon aerogels, J. Sol.-Gel Sci. Technol. 52 (2009) 56–64.
[24] T.-Y. Ying, K.-L. Yang, S. Yiacoumi, C. Tsouris, Electrosorption of ions from aqueous solutions by nanostructured carbon aerogel, J. Colloid Interface Sci. 250 (2002) 18–27.
[25] X. Li, L. Liu, Y. Zhang, S.D. Shen, S. Ge, L.C. Ling, Synthesis of nanometre silicon carbide whiskers from binary carbonaceous silica aerogels, Carbon 39 (2001) 159–165.